Acta Cryst. (1992). B48, 753–761

Charge-Density Study of Deuterated Ammonium Ferrous Tutton Salt at 85 K and Comparison with Cr^{II} and Cu^{II} Salts

BY BRIAN N. FIGGIS,* CAMERON J. KEPERT, EDWARD S. KUCHARSKI† AND PHILIP A. REYNOLDS

Chemistry Department, University of Western Australia, Nedlands, WA 6009, Australia

(*Received* 25 *March* 1992; *accepted* 28 *April* 1992)

Abstract

Diammonium hexaaquairon(II) disulfate, $(ND_4)_2[Fe(D_2O)_6](SO_4)_2$, $M_r = 412.16$. At 85 (2) K, the structure is monoclinic, $P2_1/a$, $a = 9.170$ (2), $b = 12.419$ (2), $c = 6.297$ (1) Å, $\beta = 106.69$ (1)°, $V = 686.9$ (2) Å^3, $Z = 2$, $D_x = 1.99$, $D_m = 1.96$ (2) Mg m^{-3}, λ(Mo $K\alpha$) = 0.71069 Å, $\mu = 1.497$ mm^{-1}, $F(000) = 437.6$, $R(I) = 0.018$, $wR(I) = 0.028$ for 7289 reflections. The FeO_6 octahedron is fairly regular, Fe—O(7–9) = 2.150 (1), 2.137 (1), 2.098 (1) Å respectively [mean 2.13 (3) Å], with a mean O—Fe—O angle of 90.7 (3)°. The valence-orbital population analysis gives, for Fe, the near crystal-field $3d$ configuration $d_{xz}^{1.30(2)}$ $d_{yz}^{1.43(2)}$ $d_{xy}^{1.40(2)}$ $d_{x^2-y^2}^{1.22(2)}$ $d_{z^2}^{0.98(2)}$. The near equality of the t_{2g} and e_g populations respectively contrasts, as expected, with the results from the Jahn–Teller-distorted Cr^{II} and Cu^{II} cases. The M $3d$ populations follow the expectations of crystal-field and/or local-density functional calculations moderately well. When the results for all three metals are compared the charges deduced for the M, D_2O, S, SO_4 and ND_4 units are found to be reduced by about 35% from the formal values. The charges and populations in sulfate and hexaaquametal(II) ions differ in the Cu^{II} case from those of Fe^{II} and Cr^{II}. The differences indicate greater charge transfer from sulfate to hexaaquametal(II) ion *via* hydrogen bonding for Cr^{II} and Fe^{II}. This transfer is driven by the need to partly fill empty metal $3d$ t_{2g} orbitals in Cr^{II} and Fe^{II}, orbitals which are full in Cu^{II}. This comparison strengthens belief in the reliability of valence features in transition-metal complexes deduced from X-ray data.

Introduction

In this paper we continue a study of the spin and charge densities in the archetypal hexaaquametal(II) ions of the transition series, $M(OH_2)_6^{2+}$, in the ammonium Tutton salts, $(NH_4)_2M(SO_4)_2.6H_2O$. Previously, we reported charge-density results on the strongly Jahn–Teller-distorted cases of d^4 Cr^{II} (Figgis, Kucharski & Reynolds, 1990) and d^9 Cu^{II} (Figgis, Khor, Kucharski & Reynolds, 1992) with B_g ground terms formed from the formal E_g terms of cubic symmetry. Here we treat the d^6 Fe^{II} salt, where the cubic field ground term is $^5T_{2g}$ and the geometric (Figgis, Kucharski, Reynolds & Tasset, 1988) and electronic (Doerfler, 1987) departures from formal cubic symmetry are known to be minor. The study of the spin densities, using polarized neutron diffraction (PND), has covered the d^3 V^{II} (Deeth, Figgis, Forsyth, Kucharski & Reynolds, 1988), d^4 Cr^{II} (Delfs, Figgis, Forsyth, Kucharski, Reynolds & Vrtis, 1991), d^5 Mn^{II} (Fender, Figgis, Forsyth, Reynolds & Stevens, 1986), d^6 Fe^{II} (Figgis, Forsyth, Kucharski, Reynolds & Tasset, 1990) and d^8 Ni^{II} (Fender, Figgis & Forsyth, 1986) cases. We have also undertaken *ab initio* theoretical calculations which address the spin and charge densities in the ions from M = V to M = Zn (Chandler, Christos, Figgis, Gribble & Reynolds, 1992; Chandler, Christos, Figgis & Reynolds, 1992).

In common with most of the other members of the series, ammonium ferrous Tutton salt has been studied by a variety of physical methods. They include for this instance specific heat (Hill & Smith, 1953; Gill & Ivey, 1974), inelastic neutron scattering (Svare & Otnes, 1983), far IR magnetic resonance (Doerfler, Allan, Davis, Pidgeon & Vass, 1986), magnetic susceptibility (Ohtuska, Abe & Kanda, 1957; Richardson & Sapp, 1958; Sapp, 1959; Figgis, Lewis, Mabbs & Webb, 1967; Gerloch, Lewis, Phillips & Quested, 1970; Gregson & Mitra, 1972) and Mössbauer spectroscopy (Ingalls, Ono & Chandler, 1968; Gibb, 1974; Merrithew & Guerrara, 1974; Doerfler, Leupold, Nagy, Ritter, Spiering & Zimmermann, 1983). The results of many of these measurements have been accounted for by a crystal-field-based theory (Doerfler, 1987). This theoretical description of the ground state consists of the perturbation of a $^5T_{2g}$ term by spin-orbit coupling, a small rhombic ligand-field component, and a change in the effective orbital angular momentum operator, by a factor k. This is illustrated in Fig. 1. The presence of the higher lying ^5E_g cubic ligand-field term is ignored, as is covalence in the binding to the oxygen ligand

* Author for correspondence.

† Present address: CSIRO Division of Geomechanics, 39 Fairway, Nedlands, WA 6009, Australia.

0108-7681/92/060753-09$06.00

atoms, apart from its effect on k. The effects of the perturbations can be summarized as the wavefunction.

$$\psi = 0.757/d_{xy}> + 0.432/d_{xz}> - 0.489/d_{yz}> \ldots (1)$$

where z is along the Fe—O(8) bond and x is in the O(7)—Fe—O(8) plane. This wavefunction corresponds, roughly, to a cigar of spin and charge density through a pair of faces of the MO_6 octahedron.

However, the PND experiment (Figgis, Forsyth, Kucharski, Reynolds & Tasset, 1990), which reflects the ground state of the Fe^{II} ion in great detail, has features not accounted for by this treatment. It shows that covalence in the $Fe(OH_2)_6^{2+}$ ion is quite important and so are spin-polarization effects. Also, the occupation of $4s/p$ orbitals is by no means negligible. These considerations show that there are limitations of Doerfler's theory; in particular that the magnitude, shape and orientation of the spin density are more complex than the cigar through MO_6 octahedral faces.

The charge-density studies on the Cr^{II} and Cu^{II} salts, and the PND study of the former, reflect strongly the effects of the Jahn–Teller distortions: there is very appreciable covalence in the four short M—O bonds forming a square plane, but very little in the two long ones perpendicular to that plane. There is evidence of the expected difference in charge flow into or out of the $3d_\sigma$ and $3d_\pi$ metal orbitals. For Cr^{II}, where no $3d$ orbital is formally filled, both the σ and π systems feed electrons onto the metal atom. For Cu, the π-symmetry $3d$ orbitals are formally filled and they donate to the ligands, but the formally half-filled σ-type $d_{x^2-y^2}$ orbital accepts from them.

The Fe^{II} case should be distinctly different from those of Cr^{II} and Cu^{II}, firstly because of the absence of the large Jahn–Teller distortion and secondly because of the intermediate degree of filling of the $3d_\pi$ (4 e) and $3d_\sigma$ (2 e) orbitals may lead to different charge flows. One may expect a more or less equal degree of covalence in the three pairs of M—O bonds, and probably some acceptance into both the $3d_\sigma$ and $3d_\pi$ orbitals, but less than for the Cr^{II} case.

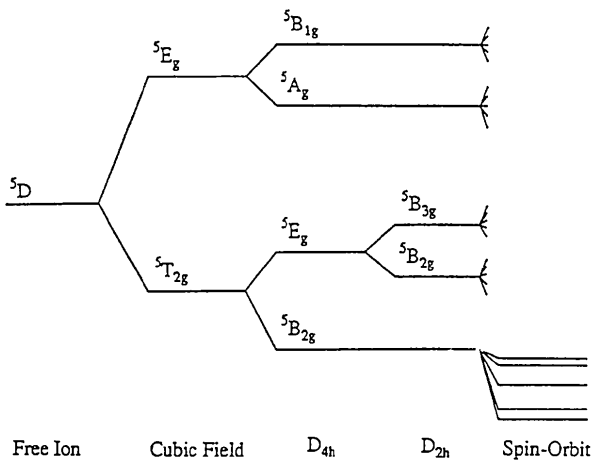

Fig. 1. Energy-level diagram for the $^5T_{2g}$ term in the presence of a low-symmetry ligand field and of spin-orbit coupling.

For experimental reasons all the PND experiments, except for the cases of Cr^{II} and Mn^{II}, were performed on deuterated crystals, as also were the charge-density studies for the Cu^{II} salt. In order to facilitate comparisons, then, we performed the present experiment on $(ND_4)_2Fe(SO_4)_2.6D_2O$. The deuteration is helpful, as it reduces the thermal motion.

Experimental

A pale-green transparent deuterated (> 98%) crystal, prepared by repeated recrystallization from D_2O, of dimensions 0.271 ($\bar{1}10$ to $1\bar{1}0$), 0.303 (110 to $\bar{1}\bar{1}0$), 0.288 (001 to $00\bar{1}$) and 0.230 mm (center to $20\bar{1}$) was mounted on a Syntex $P2_1$ diffractometer with a locally developed low-temperature nitrogen-gas-flow accessory operating at 85 (2) K. Graphite-monochromatized Mo $K\alpha$ radiation was employed. The unit cell was determined by the least-squares fitting of the setting angles of 14 well spaced reflections in the range $34 < 2\theta < 48°$. A complete sphere of data was collected with an ω–2θ scan of ω width 1.1° plus the α_1–α_2 splitting, to $2\theta = 100°$. In order to reduce the random errors in the low-angle data, of critical importance to the determination of the valence-electron distribution, this was followed by the collection of a second sphere to $2\theta = 60°$. The 228 most intense reflections were recollected with a reduced incident-beam intensity. The scan width resulted in some truncation at the highest angles, but reduced the importance of thermal diffuse scattering which may have been present. In all 49 106 data were obtained. The six standards measured after each 94 reflections showed no significant change in intensity over the period of the experiment. 3507 reflections with $I/\sigma(I) > 20$ and $I < 200\,000$ counts were used to refine the crystal dimensions so as to maximize the agreement between equivalent reflections (Figgis, Kucharski & Reynolds, 1989) after a Gaussian absorption correction, using the *XTAL* crystallographic program system (Hall & Stewart, 1990). All the data were then corrected for absorption (0.633 < transmission < 0.734) and reduced by averaging equivalents to give 7289 unique reflections with $(\sin\theta/\lambda)_{max} = 1.08$ Å^{-1}; $|h| < 20$, $|k| < 27$, $|l| < 14$, $R_{int} = 0.020$.

The details of the refinements carried out are given in Table 1.

Table 1. *Results of refinements for* $(ND_4)_2Fe(SO_4)_2.6D_2O$, *using all* 7289 *data*

	Spherical Atom	Multipole	Valence population
NP[a]	128	288	283
NVP[b]	0	214[d]	213[e]
MS[c]	–	16 (5)	15 (5)
	–	141 (23)	144 (24)
$F(000)$	409.5	436.0	437.6
Scale	12.93	12.61 (2)	12.62 (2)
$R(I)$	0.033	0.018	0.018
$wR(I)$	0.041	0.028	0.028
$R(F)$ $(F > 3\sigma)$	–	0.014	0.014
χ^{2f}	2.87	1.20	1.22

Notes: (*a*) Total number of parameters. (*b*) Number of valence parameters. (*c*) Multiple scattering parameters 1 and 2. (*d*) Includes 11 radial parameters. (*e*) Includes 10 radial parameters. (*f*) Goodness of fit.

Refinements

We employed the same model as used for the Cr^{II} (Figgis, Kucharski & Reynolds, 1990) and Cu^{II} (Figgis, Khor, Kucharski & Reynolds, 1992) salts, with only minor modification suggested by the absence of the Jahn–Teller distortion. The model incorporated anisotropic harmonic and quartic isotropic anharmonic thermal parameters on all atoms but deuterium (isotropic harmonic parameters only) and two parameters for multiple scattering (Figgis, Kucharski & Reynolds, 1989). Extinction was included initially, but found to be negligible. We used the program *ASRED* (Figgis, Williams & Reynolds, 1980). Scattering factors were calculated for valence functions from atomic wavefunctions (Clementi & Roetti, 1974) using the program *JCALC* (Figgis, Reynolds & White, 1987), except for D (Stewart, Davidson & Simpson, 1965). Core functions were taken from *International Tables for X-ray Crystallography* (1974, Vol. IV). We applied the anomalous-dispersion corrections of Kissel & Pratt (1990) modifying the work of Cromer & Liberman (1970). All 7289 data were refined to minimize the function $\sum\{\sigma(I)^{-2}[I(\text{obs}) - I(\text{calc})]\}^2$ until the maximum shift/e.s.d. was < 0.1. The final residual-density Fourier map obtained was relatively flat, with the maximum contour of 0.2 e $Å^{-3}$ occurring only at a very small region near the Fe atom, so it was not considered necessary to introduce the extensive anharmonic expansion of the Fe motion that was used in the case of the Cu^{II} salt, where the dynamic nature of the Jahn–Teller effect produces complications related to anharmonicity.

In the cases of the Cr^{II} and Cu^{II} salts, with the approximation of O_h symmetry, the formal 3*d* orbital populations can be regarded as respectively a half-filled t_{2g} shell plus an e_g electron (d^4) and the filled 3*d* shell less an e_g electron (d^9). There it was appropriate for the valence-orbital model to introduce, as well as the 3*d* orbital populations, a mixing term between the e_g members, *viz.* $\langle d_{z^2}/d_{x^2-y^2}\rangle$, to reflect the actual lower symmetry. In the present d^6 Fe^{II} instance the formal 3*d* O_h population consists of a half-filled 3*d* shell plus a t_{2g} electron. Consequently, here it is appropriate to introduce three mixing terms between the t_{2g} members, *viz.* $M(1\text{–}3) = \langle d_{xy}/d_{xz}\rangle$, $\langle d_{xy}/d_{yz}\rangle$ and $\langle d_{xz}/d_{yz}\rangle$ respectively, to reflect the actual geometry of the $Fe(OD_2)_6$ unit. On the Fe^{II} centre 4*p* valence functions were also used. sp^3hybrid orbital sets were provided on the S, N and O(7–9) atoms and *sp* hybrids plus two $2p_\pi$ orbitals on O(3–6). Bonding overlap functions, X(7–9), consisting of a Gaussian function of mean-square width 0.16 $Å^2$, were introduced at the centres of the Fe—O(7–9) bonds. Such functions, X(3–6), were also introduced in the S—O(3–6) bonds, but appeared to be so well defined that their position along the S–O bond was also allowed to refine. The fraction obtained was 0.47 (5). The effective radii of the Fe 3*d* and the S, N and O *sp*-hybrid orbitals were used as variables in the usual κ-refinement procedure (Griffin & Coppens, 1975).

The local quantization axes for the valence-orbital functions were: Fe, $z \rightarrow$ O(8), x in O(8)—Fe—O(7) plane, $y \rightarrow \sim$O(9); S, z bisecting O(3)—S—O(4), x in O(3)—O(5) plane; O(3–6), $x \rightarrow$ S; O(7–9), $x \rightarrow$ Fe, z in plane defined by Fe—O and midpoint of attached D atoms; N, $x \rightarrow$ D(11), z in D(11)–D(12) plane. $(sp^3)_1$ points along x and $(sp^3)_2$ is in the xz plane. $(sp)_1$ points along x.

The atomic coordinates and equivalent isotropic thermal parameters obtained from this refinement

Table 2. *Fractional atomic coordinates* ($\times 10^5$) *for* $(ND_4)_2Fe(SO_4)_2.6D_2O$ *at* 85 K *from the refinement*

Equivalent isotropic thermal parameters ($Å^2$) are given for Fe(1) to N(1). The isotropic quartic anharmonic parameter γ ($Å^4$) is also given for those atoms. The mid-bond density (X) parameters were fixed at one half of the distance from S to the appropriate O atom.

	x	y	z	U	γ
Fe(1)	00000	00000	00000	0.006	0.25
S(1)	41203 (1)	13085 (1)	73605 (1)	0.006	0.01
O(3)	41946 (2)	22248 (2)	58759 (4)	0.011	2.41
O(4)	55202 (3)	6737 (2)	78170 (4)	0.014	2.53
O(5)	28056 (3)	6244 (2)	62021 (4)	0.010	1.65
O(6)	38928 (2)	17312 (2)	94435 (5)	0.012	2.03
O(7)	17885 (3)	10774 (2)	17058 (4)	0.012	2.97
O(8)	−16419 (3)	11662 (2)	3014 (5)	0.012	2.41
O(9)	−116 (3)	−7090 (2)	30192 (5)	0.012	2.41
N(1)	13585 (4)	34126 (2)	35266 (6)	0.013	2.53
D(11)	8230 (80)	33070 (50)	22600 (200)	0.023 (2)	
D(12)	20700 (100)	30260 (70)	38000 (100)	0.029 (3)	
D(13)	8330 (80)	32860 (50)	43400 (100)	0.023 (2)	
D(14)	16270 (70)	40380 (70)	36800 (100)	0.027 (2)	
D(15)	21930 (70)	9230 (50)	30000 (100)	0.009 (2)	
D(16)	24830 (80)	11500 (50)	11400 (100)	0.007 (2)	
D(17)	−24140 (90)	10190 (60)	−4400 (100)	0.005 (2)	
D(18)	−14710 (70)	18060 (60)	−100 (100)	0.006 (2)	
D(19)	−8140 (80)	−6330 (60)	33600 (100)	0.005 (2)	
D(20)	1980 (80)	−13500 (60)	32500 (100)	0.008 (2)	

Table 3. *Bond lengths* (Å) *and bond angles* (°) *for* $(ND_4)_2Fe(SO_4)_2.6D_2O$ at 85 K

The values from the neutron diffraction study at 4.33 K are included for comparison.

	X-ray	Neutron		X-ray	Neutron
Fe—O(7)	2.1499 (7)	2.152 (2)	S—O(3)	1.4866 (6)	1.488 (3)
Fe—O(8)	2.1365 (8)	2.140 (2)	S—O(4)	1.4629 (6)	1.463 (3)
Fe—O(9)	2.0980 (9)	2.100 (2)	S—O(5)	1.4840 (5)	1.485 (3)
O(7)—D(15)	0.814 (8)	0.974 (2)	S—O(6)	1.4822 (7)	1.484 (2)
O(7)—D(16)	0.820 (8)	0.972 (2)	N—D(11)	0.820 (9)	1.022 (2)
O(8)—D(17)	0.822 (7)	0.980 (2)	N—D(12)	0.789 (9)	1.018 (2)
O(8)—D(18)	0.844 (7)	0.975 (3)	N—D(13)	0.812 (8)	1.028 (2)
O(9)—D(19)	0.829 (8)	0.977 (2)	N—D(14)	0.812 (8)	1.032 (2)
O(9)—D(20)	0.821 (7)	0.981 (3)			
Hydrogen bonds					
D(15)—O(5)	1.968 (8)	1.807 (2)	D(20)—O(3)	1.890 (7)	1.738 (3)
D(16)—O(6)	2.031 (8)	1.880 (2)	D(11)—O(6)	2.115 (8)	1.927 (2)
D(17)—O(4)	1.872 (7)	1.714 (2)	D(13)—O(3)	2.105 (8)	1.877 (2)
D(18)—O(6)	1.896 (7)	1.766 (3)	D(14)—O(5)	2.034 (4)	1.819 (3)
D(19)—O(5)	1.924 (8)	1.781 (2)			
O(7)—Fe—O(8)	89.41 (4)	90.4 (1)	O(3)—S—O(4)	109.88 (3)	109.7 (1)
O(7)—Fe—O(9)	90.58 (3)	90.4 (1)	O(3)—S—O(5)	107.85 (3)	107.8 (1)
O(8)—Fe—O(9)	90.97 (2)	91.1 (1)	O(3)—S—O(6)	109.21 (4)	109.2 (2)
Fe—O(7)—D(15)	114.6 (5)	113.5 (2)	O(4)—S—O(5)	109.34 (4)	109.7 (2)
Fe—O(7)—D(16)	115.3 (5)	115.2 (2)	O(4)—S—O(6)	110.83 (2)	110.9 (1)
Fe—O(8)—D(17)	113.2 (5)	113.4 (2)	O(5)—S—O(6)	109.68 (3)	109.5 (1)
Fe—O(8)—D(18)	115.7 (5)	116.0 (1)	D(11)—N—D(12)	109.9 (7)	111.5 (1)
Fe—O(9)—D(19)	115.0 (5)	114.3 (1)	D(11)—N—D(13)	106.6 (8)	107.3 (1)
Fe—O(9)—D(20)	120.2 (5)	119.6 (1)	D(11)—N—D(14)	110.1 (6)	108.6 (2)
D(15)—O(7)—D(16)	105.8 (7)	108.0 (1)	D(12)—N—D(13)	110.5 (8)	109.7 (2)
D(17)—O(8)—D(18)	107.1 (6)	106.4 (2)	D(12)—N—D(14)	110.6 (8)	109.8 (1)
D(19)—O(9)—D(20)	104.2 (7)	105.3 (2)	D(13)—N—D(14)	109.0 (7)	109.9 (2)

are given in Table 2 and the principal interatomic distances and angles in Table 3.*

For reference purposes we also performed refinements using firstly a standard spherical-atom model and secondly a conventional set of multipoles. The results of these refinements are included in Table 1. They are not discussed further in detail to avoid repetition of the Cr^{II} case. The list of multipole coefficients is included in the supplementary material.

We note from Table 1 that both the multipole and the valence refinements produce substantial improvement over the spherical-atom treatment but the fits obtained in each case are almost identical. Since the multipole coefficients are not physically transparent we prefer to use the valence-orbital populations in further discussion. The multipole analysis does, however, serve to provide a reference point for the success of the valence-orbital-based refinement.

We constructed deformation and residual density maps based upon the valence-population model using the refined thermal, scale and positional parameters. We subtracted theoretical structure factors derived from, respectively, theoretical atomic and fitted model form factors from the experimental values. The maps are shown in Figs. 2 and 3 for the three hexaaquairon(II) planes containing two pairs of O atoms, and representative sulfate and ammonium ion planes. We employed a cutoff of 0.8 $Å^{-1}$ in the Fourier summation since the use of the full data set increases the noise without adding much more valence information. Away from the atomic cores the uncertainty arising from random structure-factor errors is less than 0.05 e $Å^{-3}$. This is less than other systematic errors and we do not discuss it further.

Except for the obvious effects of change in the number of 3*d* orbitals and the absence of the Jahn–Teller distortion, the fits and parameter values strongly resemble those for the Cr^{II} and Cu^{II} examples. Therefore we do not discuss various other refinements which we carried out to explore, for example, the effects of applying or removing symmetry constraints. We merely note that results were in line with those we reported in some detail for the Cr^{II} case (Figgis, Kucharski & Reynolds, 1990), except that restricting the sulfate ion to tetrahedral stereochemistry increased χ^2 slightly (1.24).

Discussion

Geometry and thermal motion

The positional parameters of the non-H atoms are slightly, but significantly, different from those of the 4.3 K neutron diffraction study (Figgis, Kucharski,

* Lists of least-squares planes for the $Fe(OD_2)_6$ unit, anisotropic thermal parameters, multipole coefficients and structure factors have been deposited with the British Library Document Supply Centre as Supplementary Publication No. SUP 55235 (32 pp.). Copies may be obtained through The Technical Editor, International Union of Crystallography, 5 Abbey Square, Chester CH1 2HU, England.

Reynolds & Tasset, 1988). However, the observed bond lengths and angles do not differ. As expected, the charge centroids of the deuterium atoms in this X-ray experiment lie 0.22 Å (N) and 0.15 Å (O) nearer to the parent atom than to the D nuclei. The hydrogen-bonding network has no unusual features relative to the other ammonium Tutton salts, but of course was much better defined by the neutron diffraction study.

The sulfate ion is distinctly trigonally distorted, with S—O(4) (1.463) appreciably shorter than the almost equal S—O(3,5,6) [average 1.484 (2) Å] bonds. This pattern was also seen clearly in the Cr^{II} but less so in the Cu^{II} salt. This may be a consequence of O(4) being involved in only a single hydrogen bond, whereas the other three sulfate oxygens share eight hydrogen bonds (Table 3).

The FeO_6 octahedron is slightly distorted, with Fe—O(7) and Fe—O(8) scarcely different [2.143 (7)] but distinct from Fe—O(9) (2.098 Å). That difference is about the same as between the short *M*—O bond pairs in the *M* = Cr and *M* = Cu salts, and is to be compared with the difference between those short and the long *M*—O bond pairs there of *ca* 0.30 Å. The O—Fe—O angles are close to 90° (average 90.7°), so that the site symmetry at Fe with respect to bonded O atoms is approximately D_{4h}.

In conformity with the neutron diffraction experiment the thermal motion is not obviously anisotropic. The parameters for the non-H atoms are fairly uniformly larger by a factor of 2.2 (3). Since the ratio of the temperatures is *ca* 20:1, the zero-point motion must be responsible for about half of the thermal motion observed in the present study.

The effective isotropic anharmonic parameters used for the non-H atoms (average 0.2 $Å^4$) are about half those obtained for the Cr^{II} salt but about twice that reported for the Cu^{II} salt, except for Cu whose

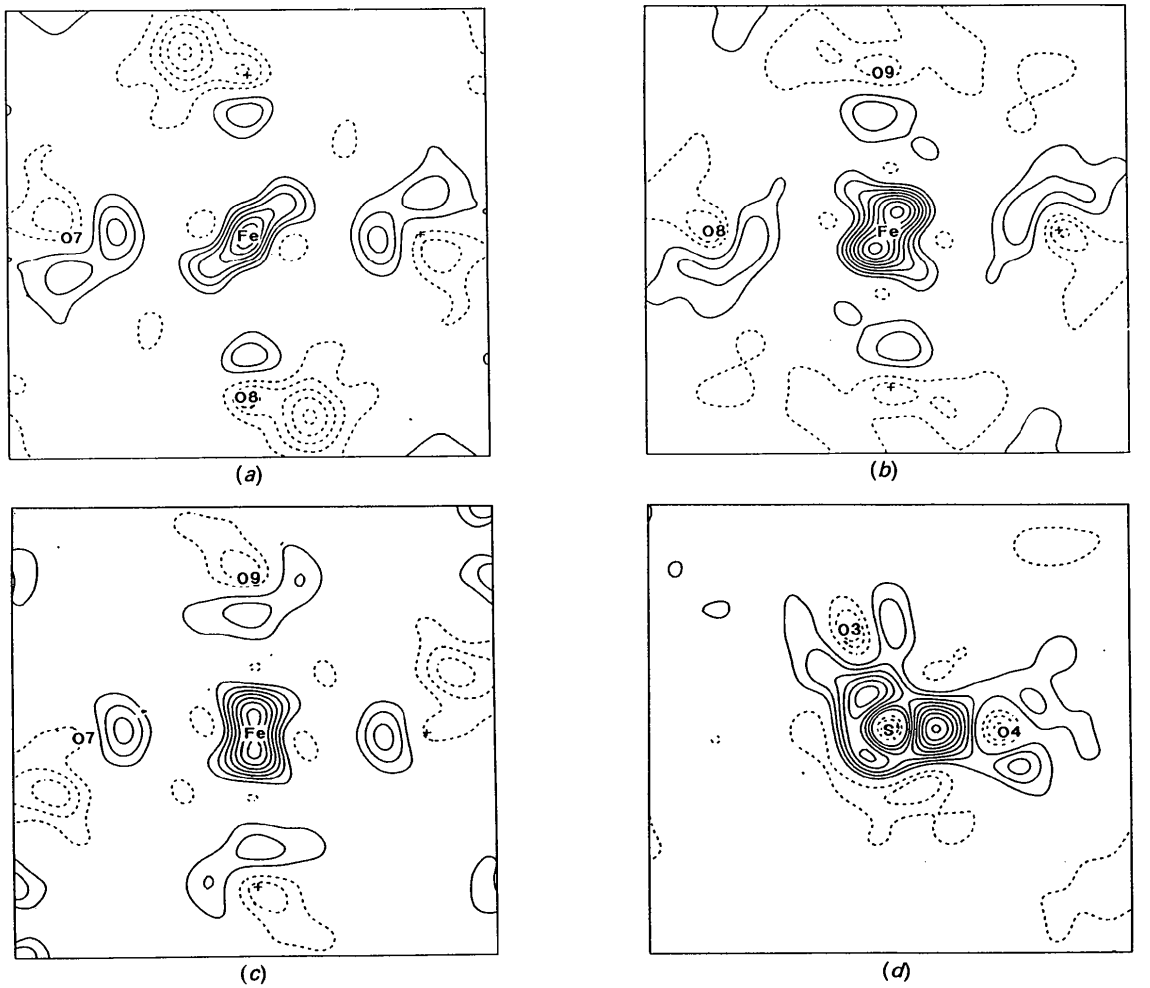

Fig. 2. Deformation density maps [$\rho - \rho$(spherical atoms)] for planes in $(ND_4)_2Fe(SO_4)_2.6D_2O$ at 85 K. The contour intervals are 0.1 e $Å^{-3}$. (*a*) Fe—O(7)—O(8) plane. (*b*) Fe—O(7)—O(9) plane. (*c*) Fe—O(8)—O(9) plane. (*d*) S—O(3)—O(4) plane.

component is large and complex as a result of the dynamic Jahn–Teller effect present. Until the origin of these parameters is better defined it is premature to comment on those differences.

Deformation and residual density maps

The deformation density maps of Figs. 2(*a–d*) show features as follows.

(*a*) Around the Fe atom (Figs. 2*a–c*) at a radius corresponding to the 3*d* orbitals, there lies a rough dumbbell of increased charge directed near to O(9), immersed in a sea of slight depletion at about the radius of the 4*p* orbitals. The dumbbell peaks at 0.7 e $Å^{-3}$. As expected, these features are much less striking than for the Cr^{II} and Cu^{II} Jahn–Teller-affected cases where the density rises to 1.1 and 1.5 e $Å^{-3}$ respectively. It appears that there is a splitting of the 3*d* t_{2g} orbital set of O_h symmetry and that the Fe atom may not have lost its more diffuse electrons to the extent expected for an Fe^{2+} ion.

(*b*) The O atoms of the water molecules, O(7–9), show evidence of lone pairs, together with a distinct depletion of density on the side away from the Fe atom. These peak at 0.3 e $Å^{-3}$, a good deal lower than for the Cr^{II} salt (0.8) but comparable with the Cu^{II} case (0.4 e $Å^{-3}$).

(*c*) On the SO_4 unit (Fig. 2*c*) there are strong movements of charge from the central regions of the atoms into the S—O bond centers. The bond-centre peaks reach 0.9 e $Å^{-3}$, a little greater than for the Cr^{II} (0.6) and Cu^{II} (0.8 e $Å^{-3}$) cases. We also see lone-pair density on the O atoms.

The model residual density maps of Figs. 3(*a–d*) are quite flat, with the strongest feature very small regions reaching 0.2 e $Å^{-3}$ near Fe. This is expected from the value of χ^2 near unity obtained from the model.

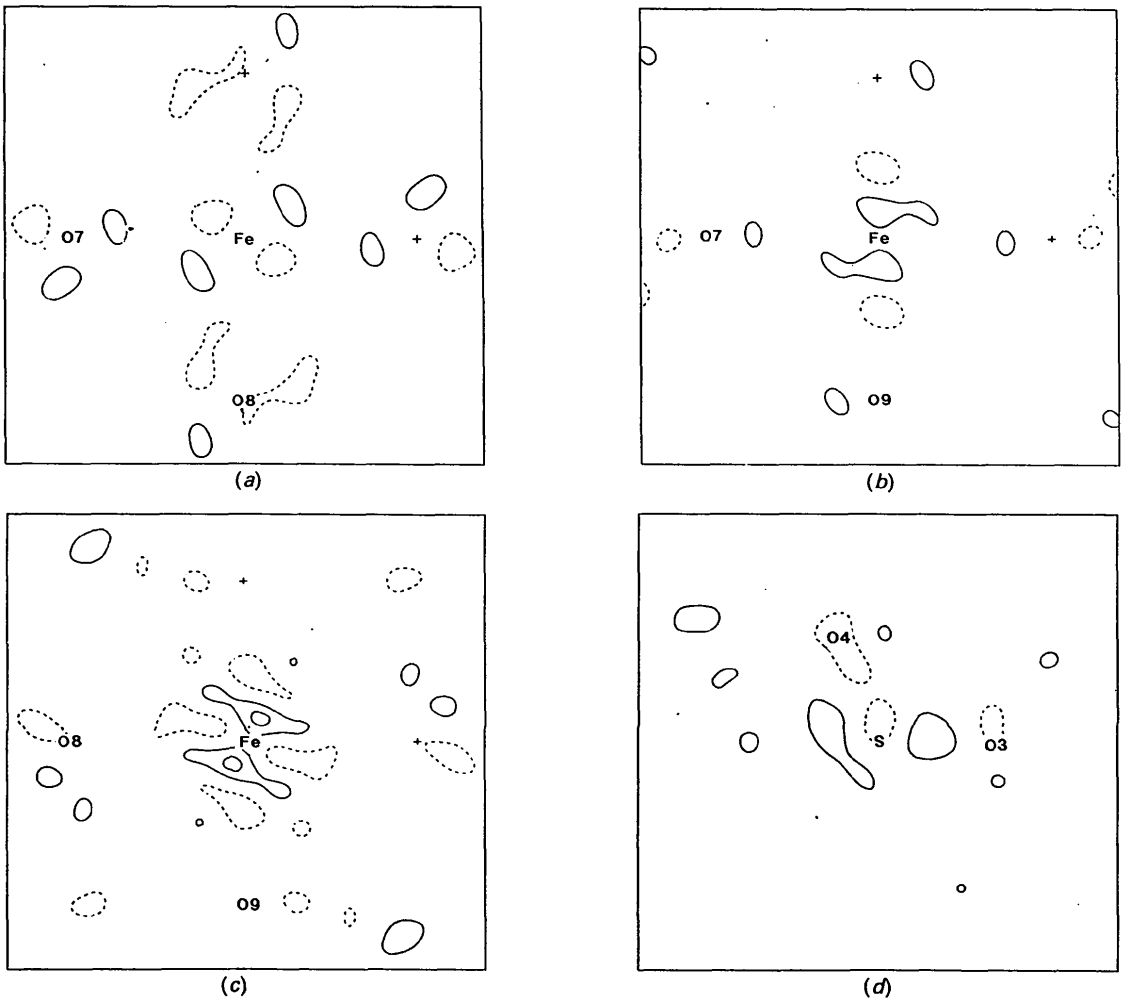

Fig. 3. Residual density maps [$\rho - \rho$(model)] for planes in $(ND_4)_2Fe(SO_4)_2.6D_2O$ at 85 K. The details are as for Fig. 2.

Table 4. *Charges obtained by using the valence-orbital population analysis for this* Fe^{II} *and the* Cr^{II} *and* Cu^{II} *ammonium Tutton salts*

The numbers in parentheses following the *M* and OD_2 entries are results from the local-density functional calculations.

	Cr	Fe	Cu
M	1.2 (2) (1.21)	0.7 (3) (1.10)	1.8 (3) (1.11)
O(7,9) (average)	−0.71 (3)	−0.46 (4)	−0.61 (3)
O(8)	−0.47 (4)	−0.57 (4)	−0.50 (4)
OD_2 (average)	0.01 (3) (0.13)	0.09 (3) (0.15)	0.00 (4) (0.14)
$M(OD_2)_6$	1.2 (2)	1.2 (2)	1.7 (2)
S	1.9 (1)	2.5 (1)	1.5 (1)
O(3–6) (average)	−0.98 (4)	−0.92 (4)	−0.96 (13)
SO_4	−1.3 (1)	−1.2 (2)	−1.5 (1)
ND_4	0.7 (2)	0.6 (2)	0.6 (2)

Population analysis

Charges on the various fragments in the structure were obtained from the valence population analysis by the procedure described for the Cr^{II} salt (Figgis, Kucharski & Reynolds, 1990). They are listed in Table 4, with the results for the Cr^{II} and Cu^{II} cases included for comparison. These charges, as is well known, have no absolute significance (Coppens, 1985). Also they have limited reliability, as they are defined by extrapolation which is often dominated by reflections at low $\sin\theta/\lambda$, which are few in number and subject to error from extinction. However, for similarly conducted and analysed experiments, they do provide a basis for comparisons.

(*a*) Fe *populations*. The transition-metal 3*d* populations are relatively well defined because they rely largely on reflections in the range of $\sin\theta/\lambda$ (0.3 to 0.7 $Å^{-1}$) for which the corrections for neither extinction nor thermal motion are large. The results of the present analysis, with averaging where suitable, are presented, along with those for the Cr^{II} and Cu^{II} salts for comparison, in Table 5. For consistency, the definition of the *xyz* coordinate system has been kept the same as for the Cr^{II} and Cu^{II} salts, so that the approximate unique axis of D_{4h} symmetry for the FeO_6 octahedron is *y*. The observed 3*d* population of 6.33 (5) suggests, as for the other Tutton salts, little covalence in the bonding involving the 3*d* orbitals. For a crystal-field model, with Fe—O(9) the short bond, we expect a 3*d* configuration of $t_{2g}^4.e_g^2$ with the t_{2g} set disturbed to increase the population of d_{xz} at the expense of $d_{xy,yz}$. The t_{2g} population, 4.13 (5) e, is indeed close to the crystal-field prediction of 4.0, but d_{xz} (1.30 e) appears to be decreased rather than increased. The disturbance of the members of the t_{2g} set is also reflected in the finite values for the mixing coefficients between them, *M*(1–3). These describe a small tilting of the quantization axes of the t_{2g} set relative to the Fe—O(7–9) framework. The e_g population of 2.20 (4) is also close to the crystal-field value of 2.0. Of the two e_g orbitals $d_{x^2-y^2}$ is close to the crystal-field prediction, but d_{z^2} is increased [1.22 (2) e] corresponding to the dumbbell of charge directed near O(9) noticed in the deformation density map. The effective 3*d* radius is unaltered from the free-ion value, in conformity with the near ionic 3*d* populations. A closer inspection of Doerfler's model shows that the prediction of the cigar of density through a pair of octahedral faces is valid only as a low-temperature limit. At temperatures of the order of a few tens of Kelvins three states are occupied leading to a 3*d* t_{2g} charge distribution which is fairly close to cubic in symmetry, as they are largely determined by the spin-orbit coupling. At 85 K, the temperature of our experiment, more states are occupied, at least partially, and we have not calculated the charge density given by the model, although it is probably closer to the lower-temperature cubic behaviour. The relative isotropy of the experimental t_{2g} populations is in conformity with this. A limitation in the applicability of Doerfler's model lies in covalence. This is observed in the PND experiment and we also observe it here. Both

Table 5. *Valence-orbital populations for units in this* Fe^{II} *and the* Cr^{II} *and* Cu^{II} *ammonium Tutton salts, averaged where appropriate*

The numbers in the lines following the *M* 3*d* populations are those from the local-density functional calculations and those predicted by an elementary crystal-field model respectively.

	Cr	Fe	Cu
M			
$3d_{xy}$	1.02 (2)	1.30 (2)	2.12 (3)
	0.98, 1.0	1.42, 1.33	1.96, 2.0
$3d_{xz}$	1.02	1.43 (2)	2.12
	0.99, 1.0	1.09, 1.33	1.96, 2.0
$3d_{yz}$	1.26	1.40 (2)	1.58
	1.00, 1.0	1.46, 1.33	1.98, 2.0
t_{2g} [a]	3.30 (6)	4.13 (5)	5.82 (10)
	2.97, 3.0	3.97, 4.0	5.90, 6.0
$3d_{x^2-y^2}$	0.28 (3)	0.98 (2)	0.82 (7)
	0.28, 0.0	1.10, 1.0	1.23, 1.0
$3d_{z^2}$	0.88 (4)	1.22 (2)	2.18 (6)
	0.99, 1.0	1.09, 1.0	1.95, 2.0
e_g	1.16 (6)	2.20 (4)	3.00 (10)
	1.27, 1.0	2.19, 2.0	3.18, 3.0
$e_g + X(7–9)/2$	1.31	2.39	3.17
4*p*	0.1 (2)	0.7 (3)	−0.2 (3)
O(*i*) (*i* = 7–9)			
$(sp^3)_1$ [b] + $X(i)/2$	1.82 (4)	1.74 (4)	1.75 (4)
$(sp^3)_2$ [c]	1.59 (2)	1.55 (2)	1.51 (2)
$(sp^3)_{3,4}$ [d]	1.62 (2)	1.60 (2)	1.65 (2)
D(15–20)	0.69 (4)	0.71 (3)	0.72 (1)
S(*i*) (*i* = 3–6)			
$(sp^3)_1$ + $X(i)/2$	1.02 (4)	0.88 (4)	1.13 (4)
O(*i*) (*i* = 3–6)			
$(sp^3)_1$ [e] + $X(i)/2$	1.70 (6)	1.88 (6)	1.59 (6)
$(sp^3)_2$ [f]	1.55 (2)	1.57 (2)	1.58 (1)
p_π	3.58 (2)	3.47 (5)	3.57 (2)

Notes: (*a*) Not really applicable to the Cr^{II} and Cu^{II} cases, on account of their Jahn–Teller distortion. (*b*) Directed at *M*. (*c*) Lone pair. (*d*) Directed at D. (*e*) Directed at S. (*f*) Directed away from S.

3*d* and 4*p* populations on the metal atoms are higher than given by an ionic model, and probably involve both *p* and *s* donation to the Fe site. In particular the high $3d_{z^2}$ population may reflect stronger σ donation.

(*b*) *The ammonium group*. This group is quite consistent across the set of metal atoms. The average N-sp^3 hybrid orbital population is 1.01 (4) e in all cases and the average D population is 1.08 (4) e, within the individual errors. The effective shortening of the N—D bonds relative to the neutron diffraction study is greater than for the O—D bonds. The reason for the almost equal N and D valence populations is not obvious. We expect a result more like that for the water molecules, where some of the D density is subsumed into that of the parent atom.

(*c*) *The water molecules*. Since covalence involving the metal 3*d* orbitals is small the expected similarity of the water molecules, except possibly for the sp^3 hybrid pointing at the metal atom, provides a test of the ability of X-ray data to describe valence effects in transition-metal complexes. Here the consistency is quite encouraging, as seen from Table 5. On O, the sp^3 hybrid directed at the metal atom, when taken with a Mulliken-type population analysis of the mid-bond density *X*(7–9), does not change within the estimated errors, having an average population of 1.77 (4) e. That is distinctly higher than for the lone pair, also consistent but outside the errors, 1.55 (4), and the hybrids directed at the D atoms, 1.62 (2) e. These latter, of course, include some of the D-atom density, the residual of which is consistent over the metal salts as 0.71 (2) e.

(*d*) *The sulfate group*. At first, we might expect that the X-ray data should provide a similar description of the sulfate group across the differing metal atoms. The results are set out in Table 5. The S-atom expectation is not well reproduced, with the average sp^3 hybrid orbital population varying by 0.25 e when the estimated error for individual metal cases is only 0.04 e. The same statement applies to the hybrid orbital on the O atoms directed at S, *viz*. $(sp)_1$. This varies by 0.28 e when the individual case errors are only 0.06 e. However, the *sum* of those populations, *viz*. $[S(sp^3)_{av} + O(sp)_1]$, 2.76 (10), 2.72 (10) and 2.72 (10) e for Fe, Cr and Cu respectively, *is* consistent. It may be that the X-ray data does not contain sufficient information to proportion the density between the S and O atoms properly although the total amount is reproduced. However, those mid-bond populations are as large, or larger, than the relevant S and O orbital populations, so that our mid-bond density with Mulliken population analysis may be too crude a model. The result may also reflect the fact that we did not attempt to model separately the π-type bonding interactions which must be present between S and O.

For the other O-*sp* hybrid and -p_π orbitals the populations are more similar. The sp_2 hybrid population, directed away from S, is unchanging [1.57 (2)], as is that of p_π [3.54 (7) e].

(*e*) *Sulfate–hexaaquametal*(II) *ion hydrogen bonding*. Comparison of the charges in the Fe^{II}, Cr^{II} and Cu^{II} cases is illuminating for the evaluation of the ability of X-ray data to reflect changes within a molecule consequent upon a perturbation in its composition. In this case the perturbation is the change in the M^{II} atom within the $M(OD_2)_6$ unit. This comparison may be more sensitive to interionic effects than the absolute charges, whose meaning is less certain. If inter-ion effects are negligible, it is expected that the charges on the SO_4 and the NH_4 units should be fairly independent of *M*, as should be those on S and N. Some small change in the charge on *M* is expected. In the series of local-density functional calculations (Chandler, Christos, Figgis & Reynolds, 1992) on $M(OH_2)_6^{2+}$ ions the charge on *M* varied only by 0.1 between the metals, as shown in Table 4. These expectations are not well met in our X-ray experiments if the estimated errors attached to the quantities are valid. The Fe^{II} and Cr^{II} cases show the same charge for the $M(OD_2)_6$ unit [1.2 (2)] but that is just significantly different from the Cu^{II} case [1.7 (2)]. Within that unit the water molecule charge for this Fe^{II} case [0.09 (3)] is just significantly different from the close Cu^{II} and Cr^{II} cases [0.01 (2)]. The charges on *M*, Fe = 0.7 (3), Cr = 1.2 (2) Cu = 1.8 (3), vary by a good deal outside the estimated errors, and by more than any reasonable expectation for isolated hexaaqua M^{II} ions.

The SO_4 unit presents a somewhat similar picture. The overall charge varies from 1.2 to 1.5, a range just outside the errors, but for the central S atom the variation is well outside them and unreasonably large.

The ND_4 unit is consistent, with a change of only 0.1, well within the estimated error of 0.2.

If we postulate significant $M(H_2O)_6\cdots SO_4$ charge transfers, both between and within the fragments, some of the discrepancies mentioned above for them can be reconciled. There appears to be a drift of charge from S to O in the sulfate ion, from the sulfate ion to the hexaaquametal(II) ion, and from the ligated water molecules to the metal(II) ion in all cases. The hexaaquametal(II) ion fragments can accept more from the sulfate ion in Cr^{II} and Fe^{II} [0.8 (2) each] than for Cu^{II} [0.3 (2)]. There is also some charge transfer to the ammonium ion, presumably also through hydrogen bonding. The water fragments accept charge from the sulfate ion and interact with the metal(II) ion in both σ and π fashions. This makes it difficult to separate intermolecular and intramolecular effects. However on the metal we note that both Cr^{II} and Fe^{II} π accept

from the water molecules [0.30 (6) and 0.13 (5)] while Cu π donates 0.18 (10) e to them. We seem to see greater electron acceptance by Cr^{II} and Fe^{II} [0.8 (2) and 1.3 (3)] than Cu [0.2 (3) e].

Overall therefore we see charge transfer *via* hydrogen bonding from the sulfate ion onto the metal(II) ion. The PND experiments lend support to this conclusion. When we have spin in the metal t_{2g} orbitals more spin appears on the water protons than isolated hexaaquametal(II) ion local-density functional calculations account for, leading to the suspicion that this excess is one consequence of the hydrogen bonding. We can understand the charge movements qualitatively if we note that the minority spin metal $3d$-t_{2g} orbitals are empty in Cr^{II}, $\frac{1}{3}$ full in Fe^{II} and filled in the Cu^{II} case. This relative electron deficiency in the Cr^{II} and Fe^{II} cases can be imagined to attract electrons from electron-rich regions, in particular the sulfate ion.

References

CHANDLER, G. S., CHRISTOS, G. A., FIGGIS, B. N., GRIBBLE, D. & REYNOLDS, P. A. (1992). *J. Chem. Soc. Faraday Trans* 2. In the press.

CHANDLER, G. S., CHRISTOS, G. A., FIGGIS, B. N. & REYNOLDS, P. A. (1992). *J. Chem. Soc. Faraday Trans.* 2. In the press.

CLEMENTI, E. & ROETTI, C. (1974). *At. Data Nucl. Data Tables*, **14**, 177–478.

COPPENS, P. (1985). *Coord. Chem. Rev.* **65**, 285–307.

CROMER, D. T. & LIBERMAN, D. (1970). *J. Chem. Phys.* **53**, 1891–1898.

DEETH, R. J., FIGGIS, B. N., FORSYTH, J. B., KUCHARSKI, E. S. & REYNOLDS, P. A. (1988). *Proc. R. Soc. London Ser. A*, **420**, 153–168.

DELFS, C. D., FIGGIS, B. N., FORSYTH, J. B., KUCHARSKI, E. S., REYNOLDS, P. A. & VRTIS, M. (1992). *Proc. R. Soc. London. Ser. A*, **426**, 417–426.

DOERFLER, R. (1987). *J. Phys. C*, **20**, 2533–2542.

DOERFLER, R., ALLAN, G. R., DAVIS, B. W., PIDGEON, C. R. & VASS, A. (1986). *J. Phys. C*, **19**, 3005–3011.

DOERFLER, R., LEUPOLD, O., NAGY, D. L., RITTER, G., SPIERING, H. & ZIMMERMANN, R. (1983). *Hyperfine Interac.* **15**, 831–836.

FENDER, B. E. F., FIGGIS, B. N. & FORSYTH, J. B. (1986). *Proc R. Soc. London Ser. A*, **404**, 139–145.

FENDER, B. E. F., FIGGIS, B. N., FORSYTH, J. B., REYNOLDS, P. A. & STEVENS, E. (1986). *Proc. R. Soc. London Ser. A*, **404**, 127–138.

FIGGIS, B. N., FORSYTH, J. B., KUCHARSKI, E. S., REYNOLDS, P. A. & TASSET, F. (1990). *Proc. R. Soc. London Ser. A*, **428**, 113–127.

FIGGIS, B. N., KHOR, L., KUCHARSKI, E. S. & REYNOLDS, P. A. (1992). *Acta Cryst.* B**48**, 144–151.

FIGGIS, B. N., KUCHARSKI, E. S. & REYNOLDS, P. A. (1989). *Acta Cryst.* B**45**, 232–240.

FIGGIS, B. N., KUCHARSKI, E. S. & REYNOLDS, P. A. (1990). *Acta Cryst.* B**46**, 577–586.

FIGGIS, B. N., KUCHARSKI, E. S., REYNOLDS, P. A. & TASSET, F. (1988). *Acta Cryst.* C**45**, 942–944.

FIGGIS, B. N., LEWIS, J., MABBS, F. E. & WEBB, G. A. (1967). *J. Chem. Soc. A*, pp. 442–447.

FIGGIS, B. N., REYNOLDS, P. A. & WHITE, A. H. (1987). *J. Chem. Soc. Dalton Trans.* pp. 1737–1745.

FIGGIS, B. N., WILLIAMS, G. A. & REYNOLDS, P. A. (1980). *J. Chem. Soc. Dalton Trans.* pp. 2339–2347.

GERLOCH, M., LEWIS, J., PHILLIPS, P. N. & QUESTED, P. N. (1970). *J. Chem. Soc. A*, pp. 1941–1955.

GIBB, T. C. (1974). *J. Phys. C*, **7**, 1001–1014.

GILL, J. C. & IVEY, P. A. (1974). *J. Phys. C*, **7**, 1536–1550.

GREGSON, A. K. & MITRA, S. (1972). *Chem. Phys Lett.* **13**, 313–315.

GRIFFIN, J. F. & COPPENS, P. (1975). *J. Am. Chem. Soc.* **95**, 3496–3505.

HALL, S. R. & STEWART, J. M. (1990). Editors. *XTAL*3.0 *Users Manual*. Univs. of Western Australia, Australia, and Maryland, USA.

HILL, R. W. & SMITH, P. L. (1953). *Proc. Phys. Soc. London Sect. A*, **66**, 228–232.

INGALLS, R., ONO, K. & CHANDLER, L. (1968). *Phys. Rev.* **172**, 295–301.

KISSEL, L. & PRATT, R. H. (1990). *Acta Cryst.* A**46**, 170–175.

MERRITHEW, P. B. & GUERRARA, J. J. (1974). *Inorg. Nucl. Chem. Lett.* **10**, 1017–1023.

OHTUSKA, T., ABE, E. & KANDA (1957). *Sci. Rep. Res. Inst. Tohoku Univ. Ser. A*, **9**, 476–491.

RICHARDSON, J. T. & SAPP, R. C. (1958). *J. Chem. Phys.* **29**, 337–339.

SAPP, R. C. (1959). *J. Chem. Phys.* **30**, 326–327.

STEWART, R. F., DAVIDSON, E. R. & SIMPSON, W. T. (1965). *J. Chem. Phys.* **42**, 3175–3187.

SVARE, I. & OTNES, K. (1983). *Physica* B, **120**, 159–162.

Acta Cryst. (1992). B**48**, 761–763

Novel High-Temperature Polymorphs of $MgBr_2$ and $MnBr_2$ – Limits of Powder Diffraction for Structure Determination

BY MICHAEL SCHNEIDER, PETER KUSKE AND HEINZ DIETER LUTZ*

Universität Siegen, Anorganische Chemie I, *W*-5900 *Siegen, Germany*

(*Received* 9 *March* 1992; *accepted* 30 *April* 1992)

Abstract

High-temperature polymorphs of magnesium bromide and manganese bromide, hexagonal, $R\bar{3}m$, Z = 3. $MgBr_2$, M_r = 184.13, Cu $K\alpha_1$, λ = 1.54051 Å, T = 973 K, a = 3.9152 (7), c = 19.420 (4) Å, V = 257.80 (9) Å^3. $MnBr_2$, M_r = 214.76, neutron radiation, λ = 1.594 (2) Å, T = 773 K, a = 3.92240 (2), c = 19.167 (2) Å, V = 255.38 (3) Å^3, Rietveld

* Author to whom correspondence should be addressed.

0108-7681/92/060761-03$06.00